Effects of Friction Stir Processing Parameters and *In Situ* Passes on Microstructure and Tensile Properties of Al-Si-Mg Casting

G.R. CUI, D.R. NI, Z.Y. MA, and S.X. LI

Friction stir processing (FSP) was applied to modify the microstructure of an as-cast A356 alloy. The effects of rotation rate, travel speed, *in situ* FSP pass, FSP direction, and artificial aging on microstructures and tensile properties were investigated. FSP broke up the coarse eutectic Si phase into 2.5 to 3.5 μm particles and distributed them homogeneously, and resulted in the dissolution of the coarse Mg_2Si particles and the elimination of porosity, thereby improving both the strength and the ductility of the casting. Increasing the rotation rate was beneficial to breaking up and dissolving the particles, but it contributed little to eliminating the porosity. The travel speed did not affect the size of the particles apparently, but lower speed was beneficial to eliminating the porosity. 2-pass FSP showed an obvious advantage in the microstructure modification and tensile properties compared with the single-pass. However, a further increase of FSP passes only resulted in slight improvement. The FSP direction of the following pass did not show distinct effect on the microstructure and tensile properties. After post-FSP artificial aging, the strengthening phase (β''-Mg_2Si) precipitated, which increased the strength and decreased the ductility of the FSP samples.

DOI: 10.1007/s11661-014-2494-8

I. INTRODUCTION

THE depletion of natural resources and the deterioration of our environment are two of the most serious problems of our current world. Using lightweight and high strength materials in fields such as the automobile manufacturing industry will help reduce resource consumption and pollution. Therefore, it is vital to incorporate high strength and high performance alloys into these industries. A356 aluminum alloy is widely used to produce automobile wheels and other parts due to its relatively good casting properties, mechanical properties, corrosion resistance, and physical properties.[1,2]

The high strength of the A356 alloy is mainly derived from the precipitation hardening of fine Mg_2Si phases,[1,2] which is dependent on heat treatment conditions.[3–5] Furthermore, the mechanical properties of the cast A356 alloy are also controlled by factors such as the volume fraction and dimension of shrinkage,[6,7] the shape and distribution of eutectic Si particles,[8,9] and Fe-rich intermetallic phases. Among these, porosity is a main factor harmful to mechanical properties, particularly fatigue properties.[10,11] Furthermore, it was also reported that the strength and the crack propagation resistance of the A356 alloy would benefit from the refinement of dendrites and the uniform distribution of Si particles.[12–15]

In order to enhance the mechanical properties of A356 castings, it is necessary to modify the microstructure. However, traditional solutions through chemical modification or heat treatment[1,7,16,17] have their particular limits. For example, chemical modification would introduce defects at high temperature or unsustainable modification effect; whereas heat treatment could not exert effect on the pores. Recently, the technique of friction stir processing (FSP), a development based on friction stir welding (FSW),[18] has been demonstrated to be effective in overcoming the above shortcomings.

It was reported that FSP on the casting materials resulted in the breakup of brittle secondary phases, the refinement of matrix grains, the dissolution of precipitates, and the elimination of porosity, thereby significantly improving the mechanical properties of cast alloys.[19–28] For cast A356 alloy, FSP has been demonstrated to produce significant enhancement of tensile properties[22,23]: the yield strength (YS), ultimate tensile strength (UTS), and total elongation was 132, 169 MPa, and 3 pct for the as-cast sample and 168, 264, and 31 pct for the FSP sample, respectively. In particular, the combined effects of travel speed (51 to 203 mm/min), rotation rate (300 to 1100 rpm), tool shapes, and 2-pass FSP on the microstructure evolution and mechanical properties of cast A356 alloy have been investigated, and an important conclusion, that 2-pass FSP could further increase the mechanical properties, is drawn.[22,23]

G.R. CUI, formerly Postgraduate with the Shenyang National Laboratory for Materials Science, Institute of Metal Research, Chinese Academy of Sciences, 72 Wenhua Road, Shenyang 110016, P.R. China, is now Lecturer with the Harbin Institute of Technology at Weihai, No.2, Wenhua West Street, Weihai 264209, P.R. China. D.R. NI, Associate Professor, and Z.Y. MA and S.X. LI, Professors, are with the Shenyang National Laboratory for Materials Science, Institute of Metal Research, Chinese Academy of Sciences. Contact e-mail: zyma@imr.ac.cn

Manuscript submitted January 17, 2014.
Article published online August 14, 2014

However, the investigated FSP parameters were limited to relatively low rotation rates and travel speeds. Furthermore, for 2-pass FSP, only one set of FSP parameters (rotation rate: 900 rpm, travel speed: 203 mm/min) was examined. Considering that an increase in the number of FSP passes and the rotation rate would induce more intensive deformation and thermal cycles, it is worthwhile investigating whether more FSP passes and higher rotation rates would produce better mechanical properties. On the other hand, although FSP has been proven to significantly enhance the mechanical properties of cast A356 alloy, the evolution of Mg_2Si precipitates during FSP, in particular during multi-pass FSP, and the hardening behavior during the post-FSP aging are still not well understood.

In this study, cast A356 plates were subjected to FSP under a wide range of parameters and the effects of the FSP passes and directions, as well as the post-FSP aging were examined. The aim is (a) to optimize the FSP parameters under higher rotation rates (up to 1800 rpm) and travel speeds (up to 450 mm/min), (b) to examine the effect of *in situ* FSP passes on the microstructure and mechanical properties (up to five passes), (c) to elucidate the evolution of the Mg_2Si precipitates during FSP, and (d) to investigate the effect of the post-FSP aging on the mechanical properties and fracture behavior.

II. EXPERIMENTAL

A cast A356 alloy was received in the form of $10 \times 90 \times 400$ mm cast plates. The chemical composition and tensile properties of the as-received and T6-treated A356 alloy are given in Tables I and II, respectively. The as-received and T6-treated base materials are referred to as "BM" and "BM + T6", respectively. The plates were machined into $8.2 \times 80 \times 400$ mm workpieces and subjected to FSP. An M42 tool with a concave shoulder 24 mm in diameter, and a threaded conical pin 8 mm in root diameter, 4 mm in tip diameter, and 6.8 mm in length was used. In order to investigate the effect of FSP passes on the microstructure and mechanical properties of the casting, *in situ* multi-pass FSP (with a 100 pct overlap) was conducted with up to five passes. The plates were cooled to room temperature in air between successive passes. A tool tilt angle of 3 deg was used for all FSP operations.

Table I. Chemical Composition of Cast A356 Alloy

Element	Si	Mg	Fe	Ti	Al
Weight Percentage	6.93	0.43	0.09	0.12	bal.

The FSP parameters used in this study are summarized in Table III. Based on the FSP conditions, fourteen samples were classified into four groups to evaluate the effects of rotation rate, travel speed, FSP pass, and travel direction: group A, changing the rotation rates at a given travel speed; group B, changing the travel speeds at a given rotation rate; group C, multi-pass FSP with the same travel directions; and group D, 2-pass FSP with the same and opposite travel directions, respectively. Such experimental design was based on the following considerations: (a) the parameters of rotation rate and travel speed should cover a range as large as possible without causing instability or significant defects; (b) the experiments began with changing the rotation rate at fixed travel speed (group A), and the two rotation rates were selected for their better tensile properties than the others in group A; (c) based on the above experimental results, the parameter combination of rotation rate and travel speed that brought better tensile properties was chosen in groups C and D.

After FSP, all samples received an artificial aging at 438 K (165 °C) for 5 hours, an optimized procedure based on a previous study.[22] The heat treatment conditions of the FSP samples before and after post-FSP artificial aging are referred to as "FSP" and "FSP + Age," respectively. For the sample produced at a tool rotation rate of 900 rpm and a travel speed of 150 mm/min (hereafter denoted by rotation rate/travel speed; *i.e.*, 900/150), a thermal profile during FSP was recorded by embedding a thermocouple in a region below the stirred zone (SZ). The heat evolution of the BM and samples of group C was measured using a differential scanning calorimeter (DSC) at a heating rate of 10 K/min.

Table II. Tensile Properties of Cast A356 Alloy

Condition	YS (MPa)	UTS (MPa)	UEL (Percent)	El (Percent)
As-cast	81	162	1.5	1.8
T6 (540 °C/4 h, 165 °C/5 h)	241	273	0.9	1.1

Table III. FSP Parameters Used in This Study

	A					B						C					D	
Sample	1	2	3	4	5	1	2	3	4	5	6	1	2	3	4	5	1	2
Rotation rate (rpm)	600	900	1200	1500	1800	1200	1200	1200	1500	1500	1500	1500	1500	1500	1500	1500	1500	1500
Travel speed (mm/min)	150	150	150	150	150	150	300	450	150	300	450	300	300	300	300	300	300	300
Pass	1	1	1	1	1	1	1	1	1	1	1	1	2	3	4	5	2	2-OD

Travel direction of multi-pass FSP: sample D2 in opposite directions (OD), the others in same directions.

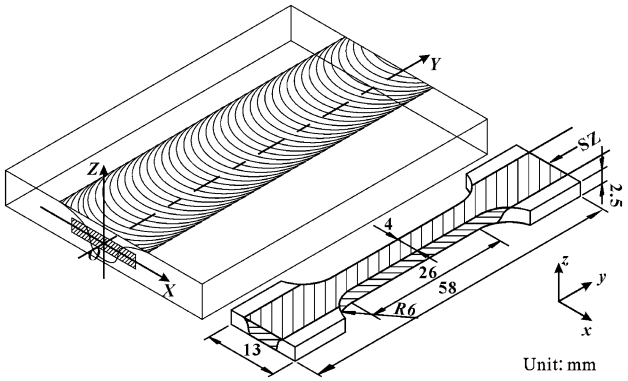

Fig. 1—Schematic illustration of sampling method and dimension of tensile specimen (tensile direction is along the OY).

Specimens for optical microscopical observation were machined from the SZ perpendicular to the FSP direction, ground with 2000 grit SiC paper and mechanically polished. ImagePro software was used to estimate the sizes of Si particles and porosities in the SZs, and only those sizes larger than 0.25 μm were brought into the statistics. For each sample, at least five pictures were taken at the center of the SZ and used for the statistics. This region is about 20 pct of the total area of the SZ and may represent the real situation. An equivalent diameter D ($D = (d_L d_T)^{1/2}$) was used to define the size of Si particles, where d_L and d_T are the dimensions of the major and minor axes of the particles, respectively. The aspect ratio of Si particles is defined as the ratio of d_L to d_T. The roundness of Si particles is defined as $R = L^2/(4\pi A)$, where L and A are the perimeter and area of Si particles, respectively.

As shown in Figure 1, tensile specimens with a gauge length of 18 mm and a width of 4 mm were cut in the SZ parallel to the travel direction and thinned to 2.5 mm thickness with the top and the bottom parts removed. The specimens were cut using an electrical discharge machine and then polished with sandpaper. Tensile tests were carried out on an Instron* 8871 tensile tester at a strain rate of 1×10^{-3} s^{-1} at room temperature. The fracture surfaces were examined by scanning electron microscopy (SEM, Quanta 600).

*Instron is a trademark of Instron Corporation, Norwood, MA.

III. RESULTS

A. *Microstructure*

The micrograph of the as-cast A356 alloy is shown in Figure 2. There were a lot of porosities in the BM (Figure 2(a)). According to the metallographic atlas, coarse (20 to 100 μm) dark gray eutectic Si, fishbone-like black Mg_2Si, and light gray Fe-rich intermetallic phases were distributed at the grain boundaries of the α-Al matrix (Figure 2(b)).

Figure 3 shows the optical micrographs in various regions of a single-pass FSP sample 1800/150. The porosities were fundamentally eliminated; meanwhile, the coarse Si particles, fishbone-like Mg_2Si, and Fe-rich particles were broken up and uniformly redistributed. The size of the Si particles in the center of the SZ was larger than that in other zones (Figure 3(e)), and some large Si particles with sizes of ~20 μm were observed. Furthermore, while the direction of the Si particles was basically stochastic in the center of the SZ, the Si particles in the zones away from the center (retreating side, advancing side, upper and lower zones) tended to arrange their longitudinal axis along the arc as indicated (Figures 3(a) through (d)).

The optical micrographs of the multi-pass FSP samples (group C) taken at the center of the SZ are shown in Figure 4. It seems that the quantity and size of the Si particles changed with increasing FSP passes (Figures 4(a) through (e)). At a higher magnification, it was found that in addition to the Si particles, a small number of Fe-rich phases and Mg_2Si particles also existed in the single-pass sample, and these Mg_2Si particles still retained the primary fish-bone pattern (Figure 4(f)).

Table IV shows the statistical measurements of the particles and porosities in various FSP samples. The following observations can be made. First, all FSP parameters induced a significant decrease in the volume fraction of the porosities and the sizes of the Si particles and pores. Second, in group A, as the rotation rate increased, the size of the Si particles decreased and the roundness of the Si particles also decreased except for sample 600/150; however, the aspect ratio did not show a distinct changing trend with the rotation rate. Third, in group B, as the travel speed increased, the size of the particles decreased except for sample 1500/300, but the aspect ratio and the roundness increased except for sample 1200/300, and the size and volume fraction of the porosities increased slightly except for sample 1500/300. Fourth, in group C, the size and shape of the particles hardly changed with increasing the number of FSP passes, whereas the size and volume fraction of the porosities showed a reducing trend except for the four-pass FSP sample. Fifth, in group D with the following FSP pass in the opposite direction, the size and roundness of the Si particles changed slightly, but the volume fraction of the porosities apparently decreased. It should be pointed out that although the statistical data in Table IV showed fluctuations to a certain degree due to measurement errors, the results indicate that FSP could consistently reduce the volume and size of the Si particles and porosities.

To understand further the effect of multi-pass FSP on the breakup of Si particles, the frequency distribution of the Si particle area in group C is carefully analyzed (Figure 5). In general, increasing the FSP passes slightly shifts the distribution of the Si particles to a smaller size range, but the effect is very limited.

B. *Differential Thermal Analyses*

Figure 6 shows the DSC curves of the as-cast A356 alloy and the multi-pass FSP samples (group C,

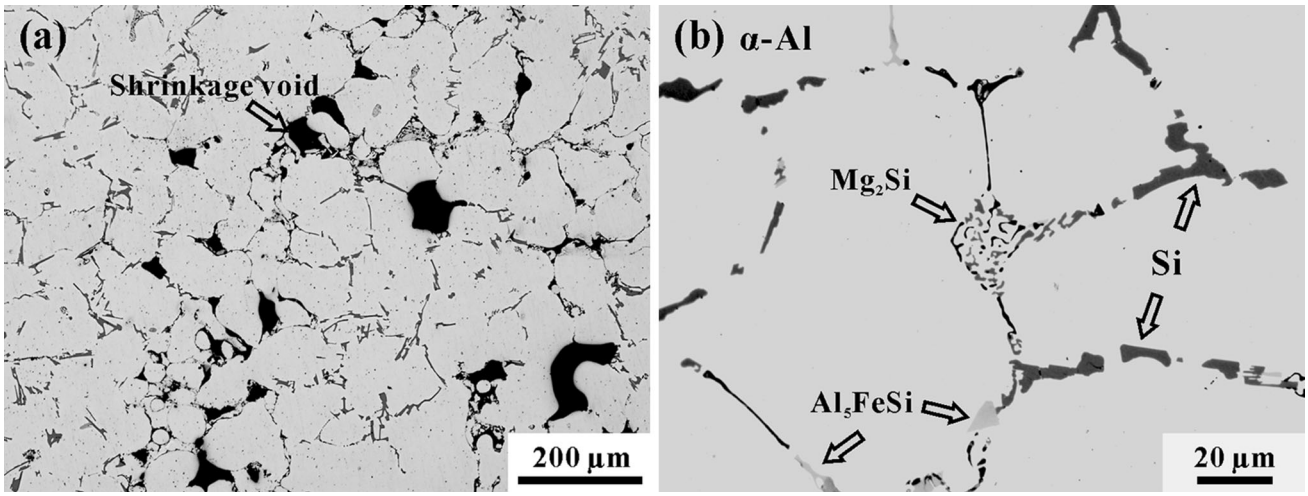

Fig. 2—Microstructure of cast A356 alloy showing (*a*) shrinkage voids and (*b*) secondary phases.

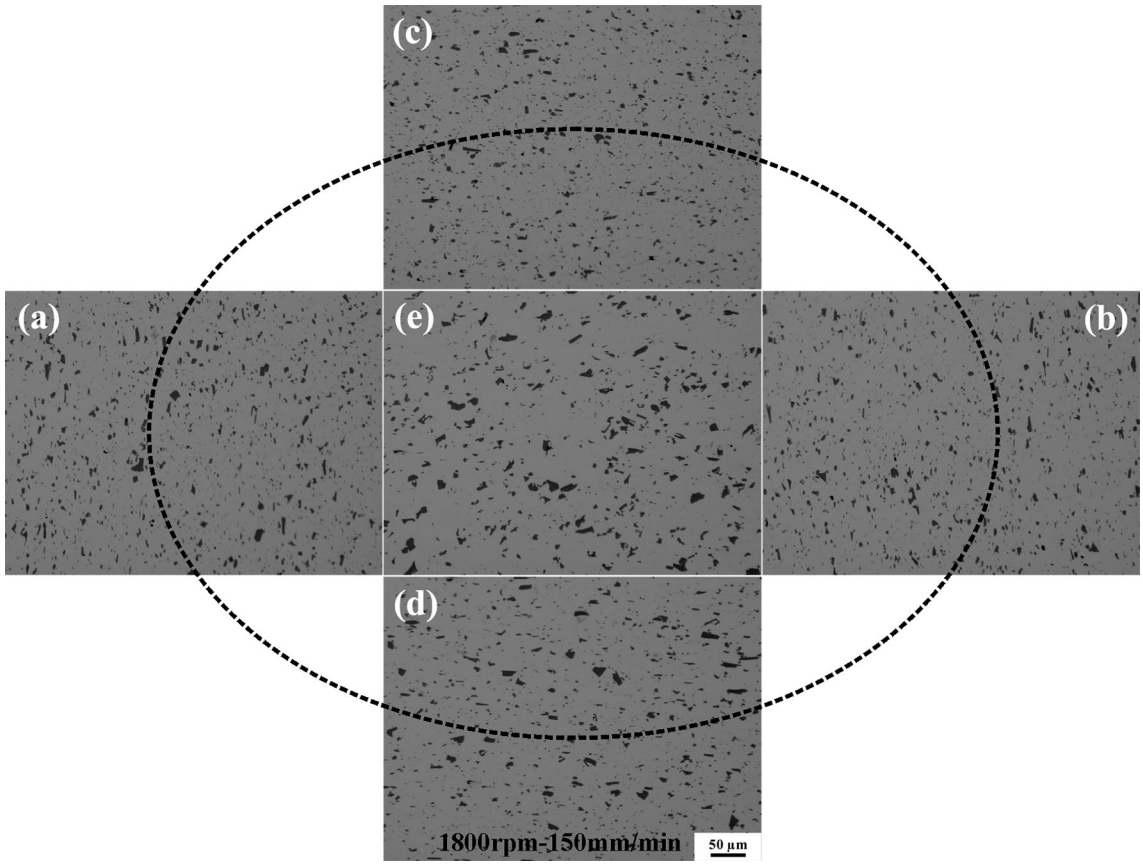

Fig. 3—Microstructure of different parts in SZ of single-pass FSP sample (group A, 1800/150): (*a*) retreating side, (*b*) advancing side, (*c*) upper, (*d*) lower, and (*e*) center.

1500/300) with the FSP passes of 1, 2, and 5. As can be seen, most curves had two precipitation peaks corresponding to β''-Mg_2Si phase and β'-Mg_2Si phase, respectively. The first peaks were located at 545 K, 539 K, 530 K, and 526 K (272 °C, 266 °C, 257 °C, and 253 °C), respectively, for the BM, single-pass, 2-pass, and 5-pass FSP samples, and their start temperature did not show significant difference among all the curves. Meanwhile, the first peak in the 5-pass FSP sample was slightly higher than that in the 2-pass FSP sample, but far higher than that in the single-pass sample, and all these peaks were apparently higher than that in the BM. The second peaks were at 665 K, 599 K, and 607 K (392 °C, 326 °C, and 334 °C) for the BM, 2-pass, and

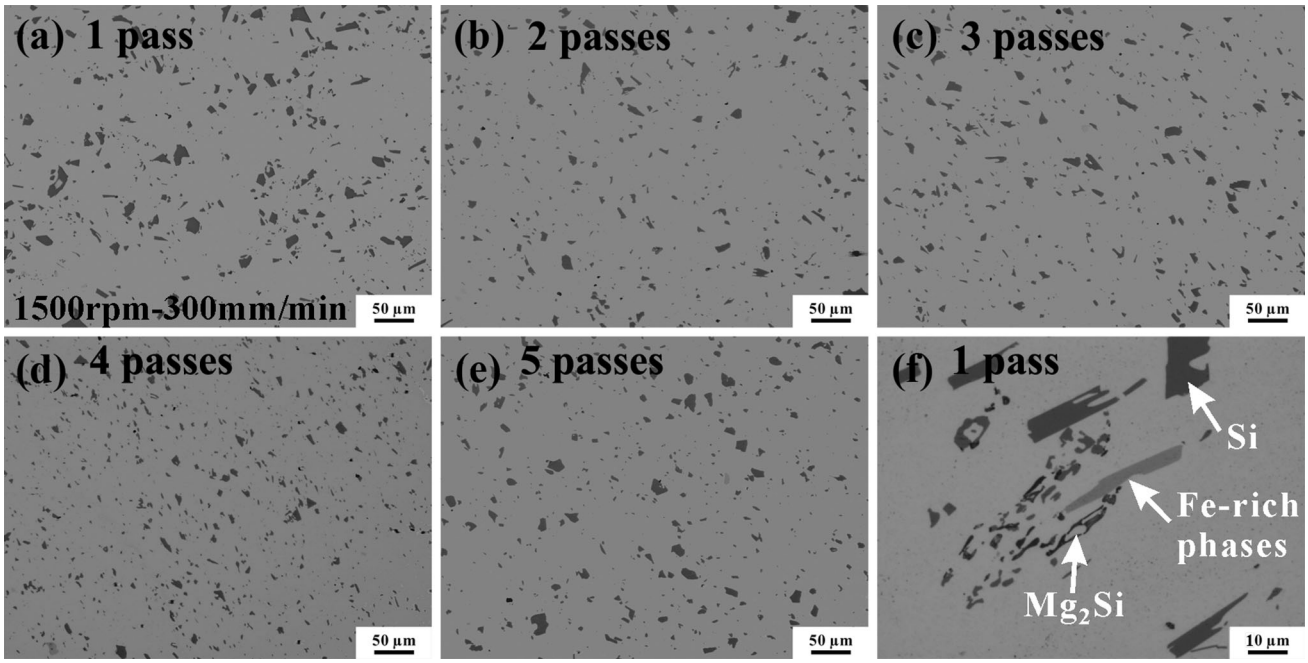

Fig. 4—Microstructure of the center of multiple-pass FSP samples (group C, 1500/300): (*a*) through (*e*) corresponding to 1-pass to 5-pass, (*f*) corresponding to 1-pass.

Table IV. The Area Content, Equivalent Size, Aspect Ratio, Roundness, Length, Width of Si Particles, and the Volume Fraction of Porosity in FSP and As-cast A356 Samples (Sample D2 in Opposite Directions (OD), the Others in Same Directions)

Sample	Rotation Rate (rpm)/Travel Speed (mm/min)	Particle				Porosity	
		Max Length (μm)	Size (μm)	Aspect Ratio	Roundness	Max Length (μm)	Vol. Pct
A							
1	600/150	31.17	3.49 ± 2.75	2.12 ± 1.06	1.89 ± 0.84	7.19	0.014
2	900/150	32.16	3.17 ± 2.83	2.02 ± 0.96	1.95 ± 1.02	13.78	0.072
3	1200/150	33.28	3.09 ± 2.69	1.88 ± 0.92	1.92 ± 0.94	9.69	0.077
4	1500/150	27.00	2.96 ± 2.74	1.93 ± 0.84	1.90 ± 0.88	12.38	0.072
5	1800/150	35.67	2.81 ± 2.54	2.03 ± 0.90	1.83 ± 0.85	15.83	0.076
B							
1	1200/150	33.28	3.09 ± 2.69	1.88 ± 0.92	1.92 ± 0.94	9.69	0.077
2	1200/300	36.01	2.99 ± 2.48	2.14 ± 0.98	1.99 ± 1.08	10.33	0.114
3	1200/450	39.31	2.51 ± 2.39	2.01 ± 0.93	2.37 ± 1.59	17.79	0.463
4	1500/150	27.00	2.96 ± 2.74	1.93 ± 0.84	1.90 ± 0.88	12.38	0.072
5	1500/300	45.94	3.14 ± 3.07	2.00 ± 0.99	1.97 ± 1.03	22.32	0.130
6	1500/450	40.08	2.92 ± 2.58	2.18 ± 1.15	2.17 ± 1.30	15.72	0.183
C							
1	1500/300-1p	45.94	3.14 ± 3.07	2.00 ± 0.99	1.97 ± 1.03	22.32	0.130
2	1500/300-2p	33.08	2.89 ± 2.71	2.04 ± 0.96	1.86 ± 0.85	10.81	0.049
3	1500/300-3p	31.75	3.09 ± 2.70	1.96 ± 0.82	1.74 ± 0.76	17.02	0.038
4	1500/300-4p	31.73	2.59 ± 2.02	2.19 ± 0.92	1.85 ± 0.77	8.01	0.066
5	1500/300-5p	40.67	2.97 ± 2.60	2.15 ± 0.90	1.80 ± 0.65	10.12	0.023
D							
1	1500/300-2p	33.08	2.89 ± 2.71	2.04 ± 0.96	1.86 ± 0.85	10.81	0.049
2	1500/300-2p OD	34.05	2.82 ± 2.78	1.60 ± 0.52	1.80 ± 1.07	13.13	0.028
As-cast		124.54	12.91 ± 6.79	4.65 ± 1.73	6.12 ± 4.16	110.72	2.59

5-pass FSP samples, respectively, but for the single-pass FSP sample it was not significant. Meanwhile, the start temperature of the second peaks in the 2-pass and 5-pass FSP samples was almost the same, but it was much lower than that in the BM. It was also noticed that the second peak in the 5-pass FSP sample was higher than that in the 2-pass FSP sample.

C. *Tensile Properties*

The typical tensile curves of the 5-pass FSP sample (sample C5, 1500/300) before and after artificial aging are shown in Figure 7. The curves were smooth without an obvious yield point; therefore, the YS is defined as the strength at 0.2 pct strain offsets. The FSP sample

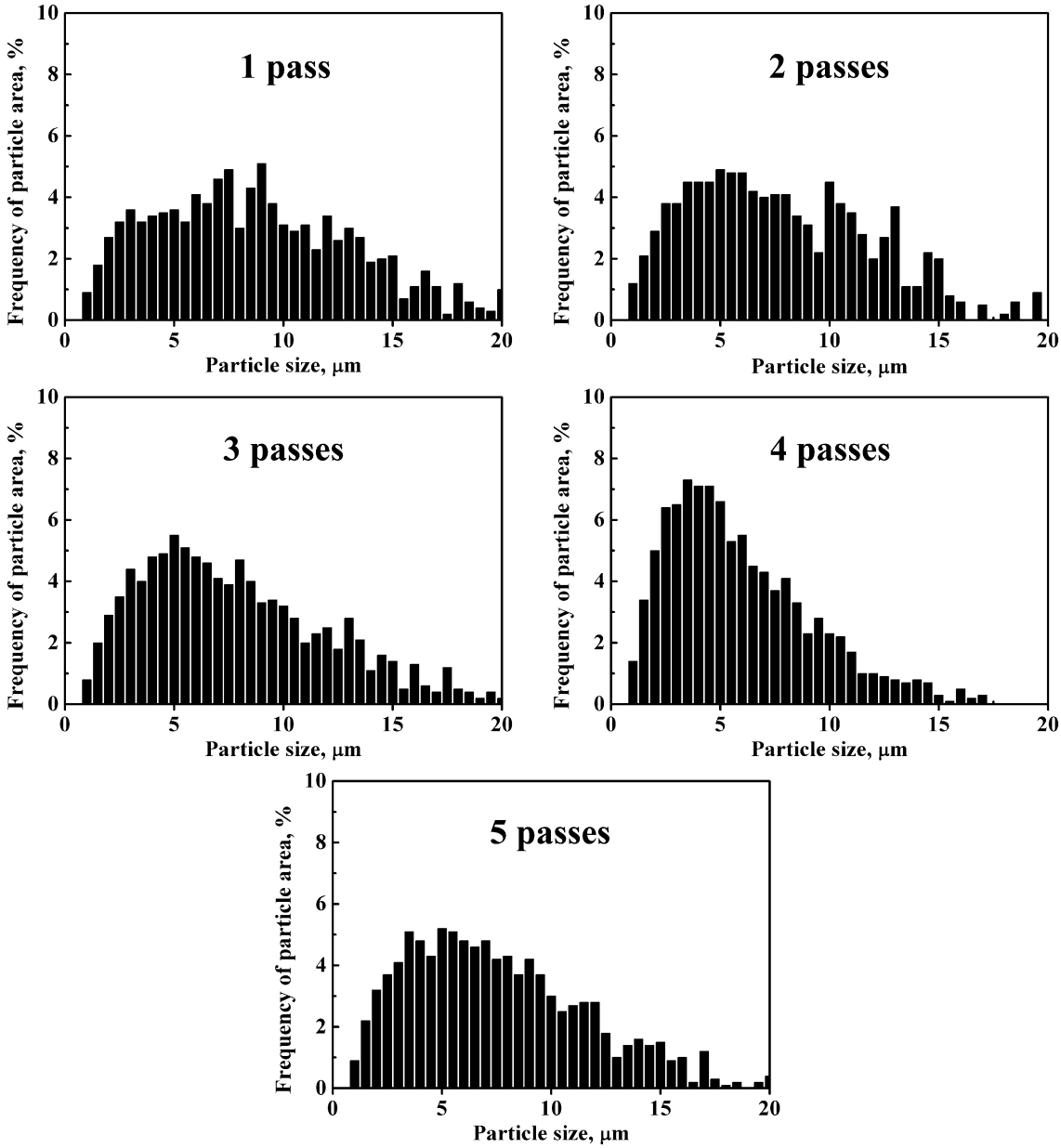

Fig. 5—Distribution of particle area against Si particle size of multiple-pass FSP samples (group C, 1500/300).

exhibited a continuous strain hardening behavior up to failure and owned an excellent uniform elongation of more than 19 pct. After aging, the FSP sample exhibited an enhanced strength and reduced ductility; however, the uniform elongation of ~7 pct was retained.

The tensile properties of single-pass FSP samples with various rotation rates at a fixed traveling speed of 150 mm/min (group A) are shown in Figure 8. While all the FSP samples exhibited higher strength and elongation than the BM (Table II), they did not exhibit a significant difference in the tensile properties with a change in the rotation rate. A close inspection reveals that at the higher rotation rates of 1500 and 1800 rpm, the FSP samples exhibited slightly decreased tensile properties. After aging, all the FSP samples exhibited increased strengths and decreased elongations, and the strength increased slightly with an increase in the rotation rate. The rotation rate of 1200 rpm resulted in an optimum combination of strength and ductility under both the FSP and the FSP + Age conditions: YS, UTS, and total elongation were 118, 223 MPa, and 19 pct for the FSP sample, and 208, 274 MPa, and 10 pct for the FSP + Age sample, respectively.

The tensile properties of single-pass FSP samples with various travel speeds at rotation rates of 1200 and 1500 rpm (group B) are shown in Figure 9. At 1200 rpm, increasing the travel speed did not show any apparent effect on the strength, whereas the elongation exhibited an obvious increase (Figure 9(a)). After aging, the strength increased but the elongation decreased; however, the tensile properties under various travel speeds were basically similar (Figure 9(b)). At

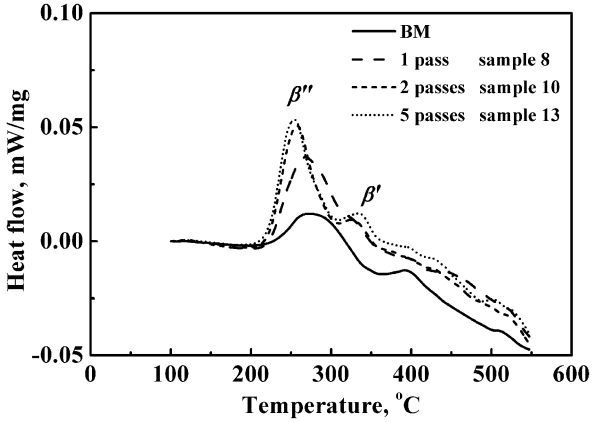

Fig. 6—DSC curves of BM and multiple-pass FSP samples (group C, 1500/300).

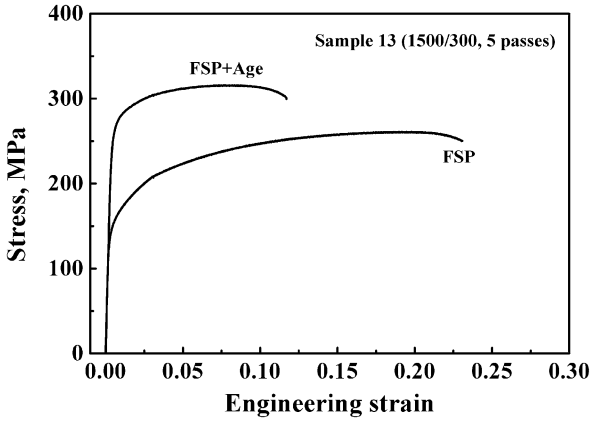

Fig. 7—Typical tensile curves of 5-pass FSP sample (group C, 1500/300).

1500 rpm, the YS increased slightly with an increase of the travel speed, and the UTS and the elongation had a peak value at 300 mm/min (Figure 9(c)). After aging, both the strength and the elongation increased and showed similar values between the three samples (Figure 9(d)).

The tensile properties of the multi-pass FSP samples with various FSP passes (group C, 1500/300, up to 5 passes) are shown in Figure 10. The strength increased but the elongation varied slightly with increasing the number of FSP passes. After aging, all the samples exhibited increased strength and decreased elongation. The 2-pass FSP sample exhibited an obvious advantage in the tensile properties compared with the single-pass sample; for the FSP + Age samples, the YS, UTS, and total elongation were 253, 305 MPa, and 11 pct for the 2-FSP sample, and 225, 278 MPa, and 10 pct for the single-pass sample. However, a further increase in the FSP passes only resulted in a slight enhancement in the tensile properties of the FSP samples.

The tensile properties of the 2-pass FSP samples with the same and opposite traveling directions (group D, 1500/300) are shown in Figure 11. The two samples showed similar strengths. With the direction opposite, the sample possessed elongation a little higher than its counterpart. After aging, the sample with the opposite direction showed a little lower strength and elongation than its counterpart.

D. *Fractography*

The typical fractographs of the single-pass FSP and FSP + Age samples at various rotation rates (group A) are shown in Figures 12 and 13. The smooth area in the dimples indicates the fractured Si particles, and the dimples without the smooth area represent the ductile rupture characteristics of the Al matrix. The size of the largest broken Si particles was about 25 μm, which is smaller than the maximum particle length, as shown in Table IV. Some fractured Si particles contained cracks indicating that the tensile fracture occurred preferentially in the area with the larger Si particles. The size of the Si particles was not uniform in the SZ and correspondingly, the fractograph showed different sizes of cracked Si particles.

IV. DISCUSSION

A. *Microstructure Evolution During FSP and Heat Treatment*

During FSP, intense plastic deformation and thermal processes induced: the elimination of porosity, the breakup and redistribution of Si particles, the refinement of grains, and the dissolution of Mg_2Si precipitates.[22] In this study, the evolution of the porosity, Si particles, and Mg_2Si precipitates were mainly considered.

Table IV indicates that FSP could fundamentally eliminate the porosity. It seems that the size and volume fraction of porosity was not obviously affected by the rotation rate (groups A and B). However, they slightly decreased with a decrease of the travel speed (group B) or an increase in the number of FSP passes (group C). For the multi-pass process, the following direction slightly affected the size and shape of the Si particles, but the opposite direction might be more effective than the same direction on the elimination of porosity (group D). In general, it could be concluded that massive deformation was necessary and effective to reduce the volume fraction of porosity. Lower travel speed increased the effect of eliminating porosity, and this can be attributed to the fact that lower travel speed could result in more material movement and thus more thorough mixing, which could effectively refine the microstructure and reduce pores.[22]

The breakup effect on particles was derived from the severe deformation and thermal cycle during FSP. The increase of rotation rate would significantly increase the strain and strain rate of deformation,[22] and this would be beneficial to the decrease of particle size (Table IV, group A). However, the situation was much more complicated for the effect of travel speed (Table IV, group B). On the one hand, the increase of travel speed reduced the strain in a unit volume and such a reduction

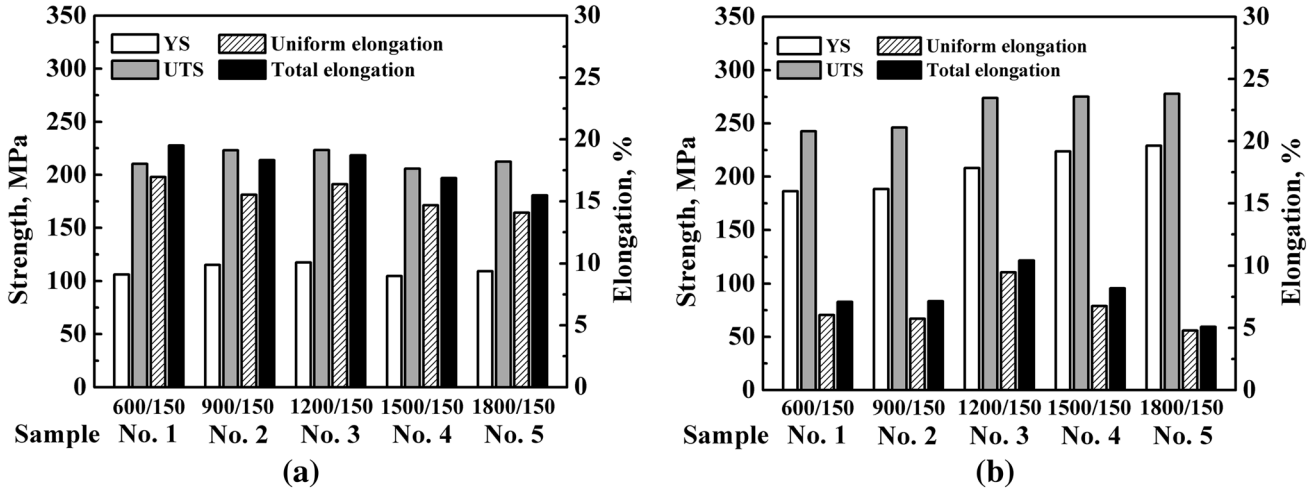

Fig. 8—Effect of rotation rate on tensile properties of single-pass FSP samples at fixed traveling speed of 150 mm/min (group A): (*a*) FSP and (*b*) FSP + Age.

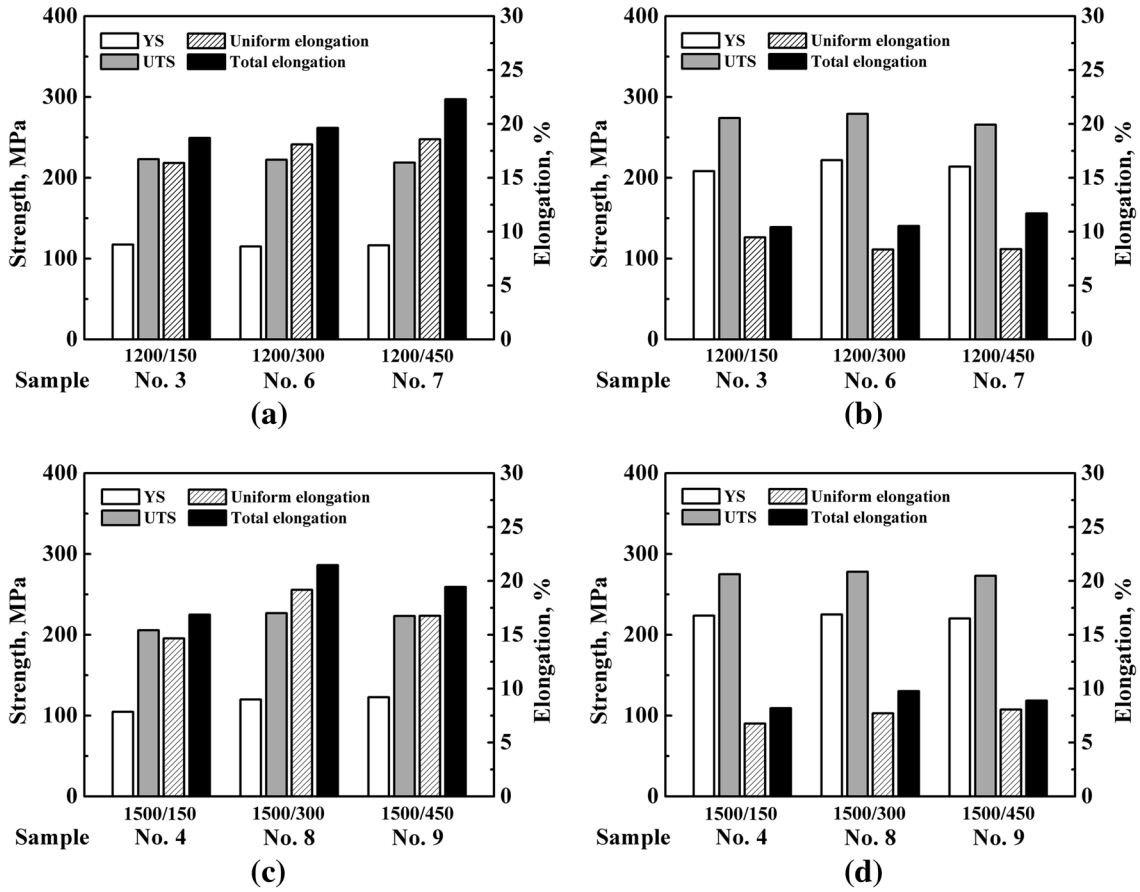

Fig. 9—Effects of travel speed on tensile properties of single-pass FSP samples (group B): (*a*) 1200 rpm, FSP; (*b*) 1200 rpm, FSP + Age; (*c*) 1500 rpm, FSP; (*d*) 1500 rpm, FSP + Age.

of plastic deformation would weaken the breakup effect of the tool. On the other hand, it means the reduction of the preheating time of the material in front of the revolving tools, and this would increase the deformation resistance of the material and promote the breakup effect on the particles. Thus, increasing the travel speed might not definitively improve or weaken the breakup effect. Consequently, the combination of travel speed and rotation rate should be optimized to produce an ideal breakup effect.

Alidokht *et al.*[29] investigated the effect of rotation rate (500 to 1250 rpm) on the FSP of an as-cast A356

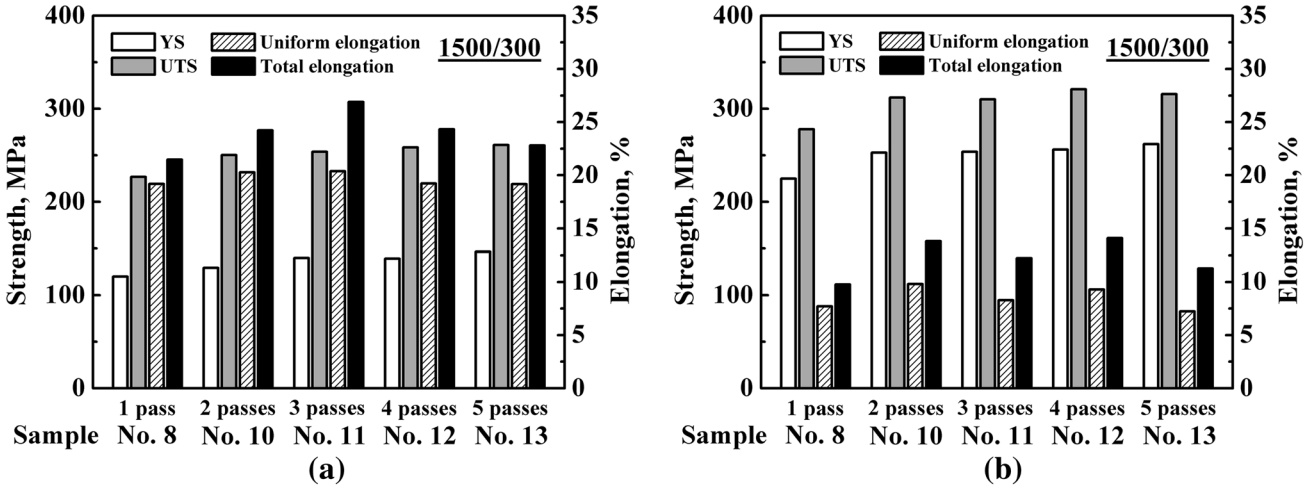

Fig. 10—Effects of FSP passes on tensile properties of multiple-pass FSP samples (group C, 1500/300): (*a*) FSP and (*b*) FSP + Age.

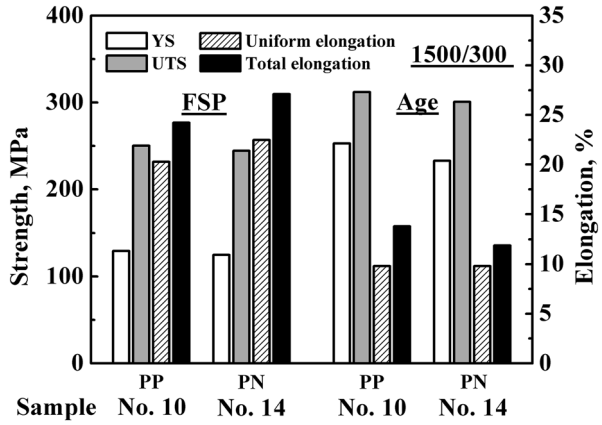

Fig. 11—Effect of second FSP direction on tensile properties of 2-pass FSP samples (group D, 1500/300).

alloy at a fixed travel speed of 50 mm/min. They reported that higher rotation rate was more effective in breaking up Si particles due to the more intense stirring effect. The result of the present study is in agreement with that of Alidokht *et al.*[29] However, this result is contrary to that reported by Mahmoud *et al.*[30]: for the FSP of an as-cast A390 alloy, the size of Si particles was reduced by reducing the rotation rate from 1800 to 1125 rpm and by increasing the travel speed from 10 to 20 mm/min.

It is assumed that the multi-pass FSP could generate a more powerful breakup effect on particles because of the repeated deformation caused by FSP. Ma *et al.*[22] reported that 2-pass FSP with 100 pct overlapping resulted in a further reduction in size and aspect ratio of Si particles and porosity level. However, the measured values of both the average particle size (Table IV, group C) and the frequency distribution of the particle area (Figure 5) in the present study indicated that increasing FSP passes did not produce a consistent particle refinement effect. Although a single-pass FSP effectively refined the coarse Si particles, increasing further the number of FSP passes to more than 2 did not result in a more obvious refinement effect. The main reason is that although the severe plastic deformation would surely exert an obvious breakup effect on the bigger particles, it might not exhibit a similar effect on the smaller particles. It was noticed that the statistical data of particles fluctuated in a certain level because the fine particles are hard to discern under optical microscopical observation.

Unlike the breakup of Si particles, heating above a critical temperature is an important factor in the dissolution of Mg_2Si particles. The usual precipitation sequence in A356 alloy is solid solution $\rightarrow$ GP zones $\rightarrow$ β''-Mg_2Si $\rightarrow$ β'-Mg_2Si. In a traditional T6 treatment, it usually takes ~4 hours at a high temperature around 813 K (540 °C) to insure the complete dissolution of coarse precipitates and the homogeneous distribution of Mg element. In order to estimate the thermal cycles in the SZs, the thermal profile of sample 900/150 (sample A2) was measured (Figure 14). The maximum temperature was 634 K (361 °C) and lasted only several seconds. This peak temperature is lower than the data in Reference 22 by about 100 K (−173 °C). The reason should be attributed to the thermocouple being embedded in the region below the SZ in this study, whereas it was placed in the thermo-mechanically affected zone (TMAZ) in Reference 22, and the temperature under the SZ was lower than that in the TMAZ.[31] Therefore, it is believed that the peak temperatures in the SZs were higher than the measured values.

Ma *et al.*[22,23] carefully examined the microstructure of as-cast and FSP A356 samples by optical, scanning electron, and transmission electron microscopy. They reported that FSP broke the fishbone-like Si into small particles, resulting in a homogeneous redistribution of the fine particles; meanwhile, high dislocation density and the interaction between fine Si particles and dislocations were observed in the FSP samples. Furthermore, most Mg_2Si particles were dissolved into the Al matrix during FSP although the dissolution process lasted for only a few seconds, which was attributed to reduced diffusion distance and accelerated diffusion rate of elements due to severe plastic deformation in

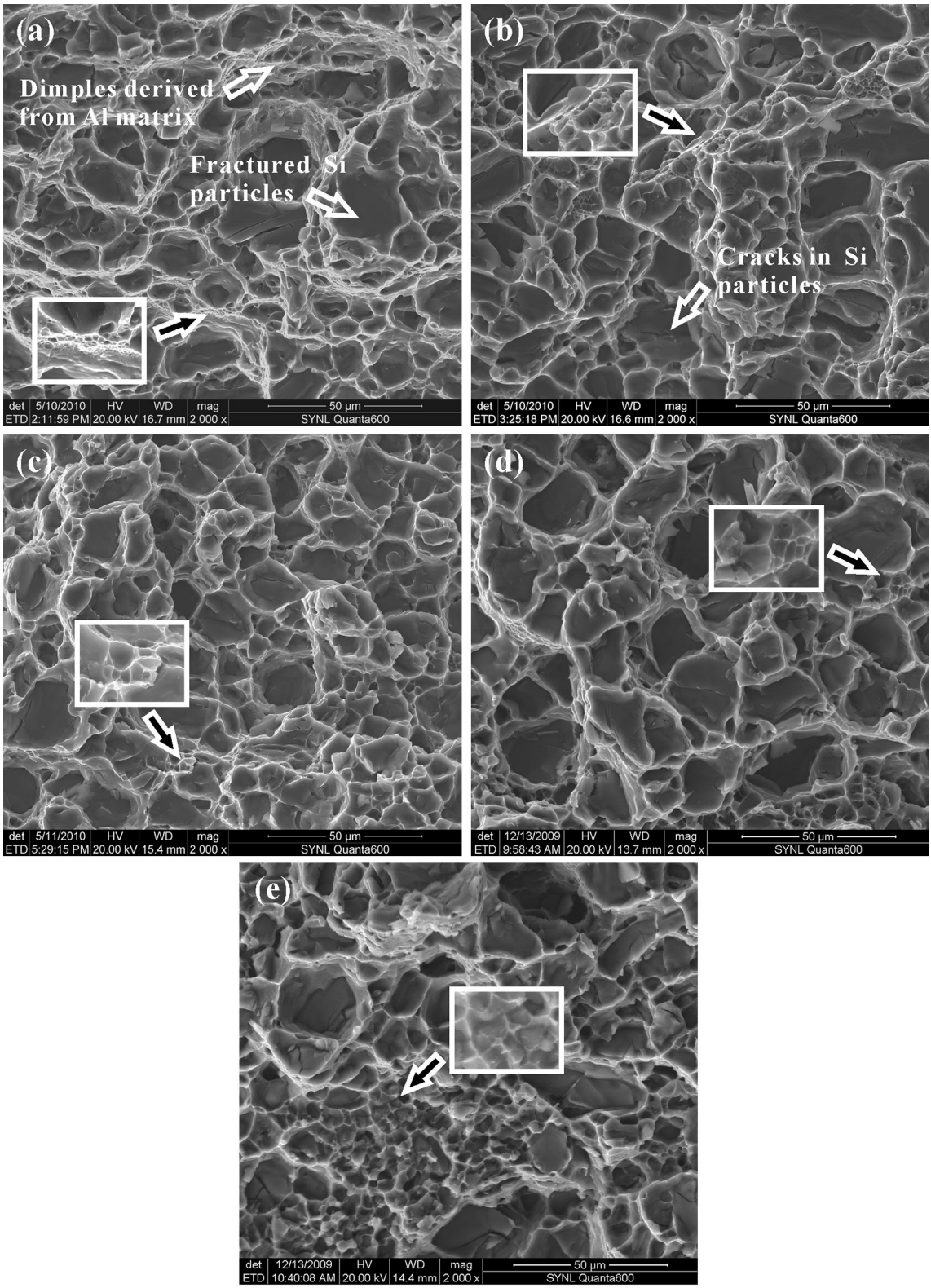

Fig. 12—Fractographs of single-pass FSP samples at various rotation rates (group A). Each inset is an enlargement of the Al dimples indicated by the arrow.

FSP.[24] Similar to those results,[22,23] the SZs in the present study showed more homogeneously distributed fine Si particles and finer Mg_2Si particles (Figures 3, 4) compared to the as-cast A356 alloy (Figure 2). However, the microstructure observations indicated that the Mg_2Si particles could not be completely broken up and

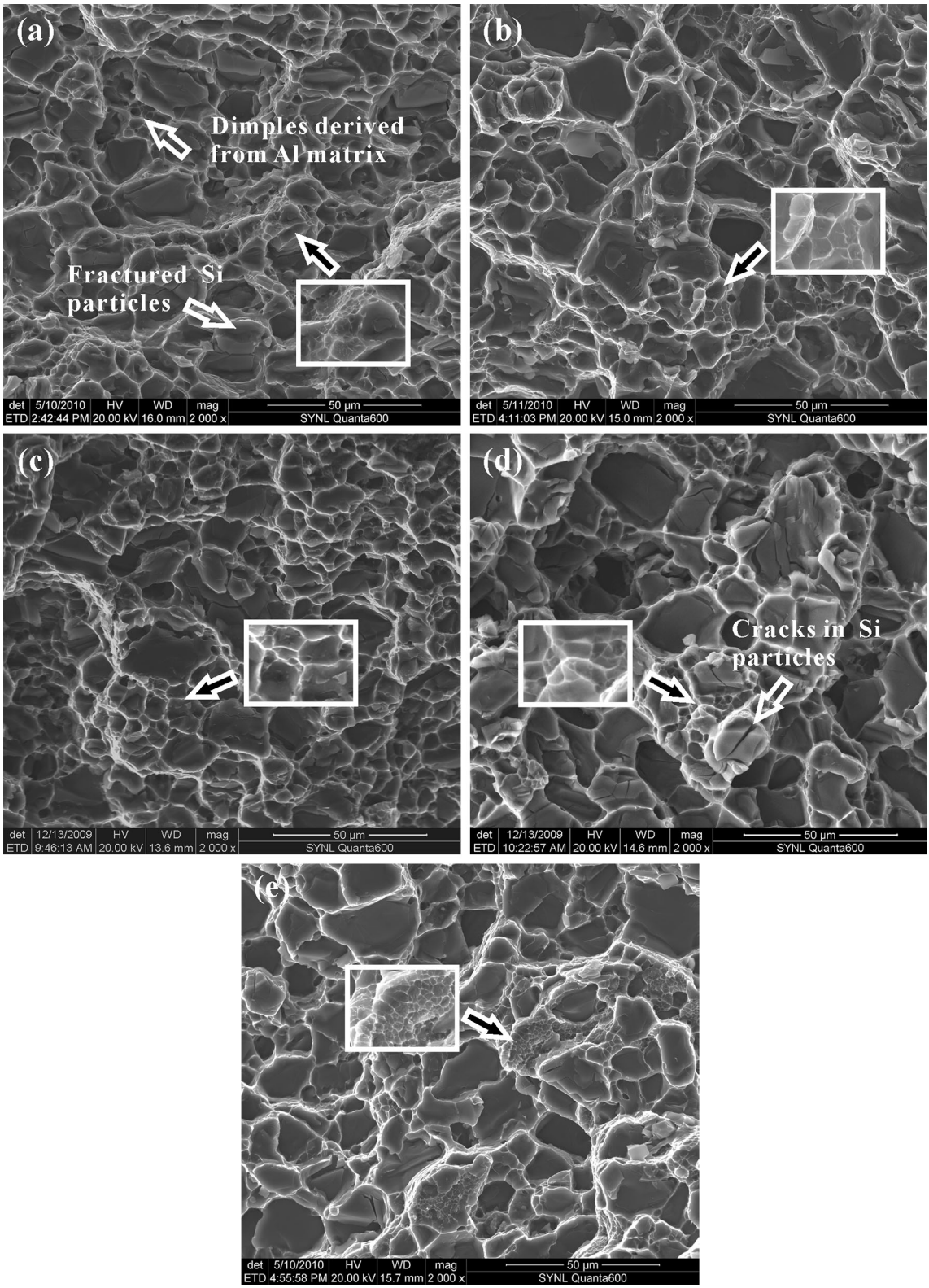

Fig. 13—Fractographs of artificial aged single-pass FSP samples at various rotation rates (Group A). Each inset is an enlargement of the Al dimples indicated by the arrow.

dissolved, even after multi-pass FSP (Figure 4(f)). This may be due to the size of the Mg_2Si being too large in the as-cast BM. Therefore, it could be concluded that FSP improved the distribution of the Mg element in the Al matrix, although not all Mg_2Si particles could be dissolved.

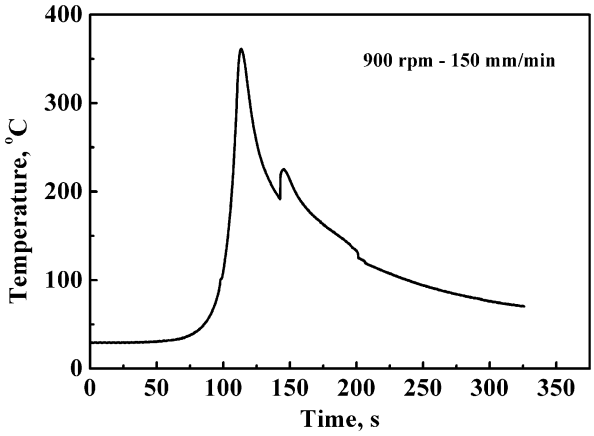

Fig. 14—Thermal profile of FSP sample (group A, 900/150).

For the multi-pass FSP, considering the fact that the FSP resulted in an increase in the strength of the BM, the process temperature of subsequent FSP passes was expected to increase due to a higher deformation resistance, which led to an increase in the amount of dissolved Mg atoms (Figure 6). A small amount of dissolved Mg atoms would precipitate as β''-Mg_2Si during every cooling process of the FSP thermal cycle in the air. In the DSC curves of the multi-pass FSP samples (Figure 6), the slight difference of the precipitation peaks of β''-Mg_2Si indicated that the amount of the remaining Mg atoms in the matrix at room temperature should be changed after each FSP pass. Moreover, the precipitation peak of β'-Mg_2Si in the 5-pass FSP sample was higher than that in the 2-pass sample. This is attributed to the transformation of more β''-Mg_2Si into β'-Mg_2Si during the DSC test.

B. *Enhancing Effects of FSP and Aging Treatment*

The feebleness of the as-cast BM is mainly attributed to the following three factors. First, many shrinkage porosities reduce the area resisting stress and are the source of cracks under deformation.[6,7] Second, the slow cooling after casting results in the generation of coarse friable eutectic Si particles,[8,9] which tend to crack under a lower stress. Third, the coarse Mg_2Si precipitates do not contribute to the strengthening of the aluminum matrix.[1,2]

The strengthening effect of FSP worked through overcoming the above three aspects.[19–24,26,28]. First, the fine recrystallized grains produced in FSP could increase the strength of the matrix.[32] The coarse Mg_2Si particles were dissolved into the α-Al matrix, promoting the strength by solution strengthening as well as precipitation strengthening due to the formation of a small amount of the β''-Mg_2Si precipitates during FSP cooling process.[22] Second, the elimination of shrinkage porosities and the breakup of eutectic Si particles reduce the possibility of crack initiation. Third, many small (<1 μm) Si particles, which might be derived from the breakup of larger Si particles or reprecipitation during the thermal cycle, should act to increase the strength due to their interaction with dislocations.[22] Meanwhile, the elongation of the FSP samples would be definitely enhanced by FSP because of the elimination of porosity and the refinement of second-phase particles.[19,20,22,24,26,28] After the post-FSP artificial aging the β''-Mg_2Si precipitated out, which increased the strength of the samples but decreased the elongation. This phenomenon is in agreement with that reported by Ma *et al.*[22]

C. *Effects of Rotation Rate and Travel Speed on Tensile Properties of Single-Pass FSP*

In group A, the strength of the FSP samples increased with an increase of the rotation rate until 1200 rpm. This is attributed to more Mg atoms being dissolved into the matrix due to higher heat input resulting from higher rotation rates.[22] However, the higher heat input could simultaneously reduce the amount of ultrafine Si particles, which was supposed to partially contribute to the strength. Thus, it is reasonable that the strength of the FSP samples did not increase monotonically with an increase of the rotation rate in the present study. This indicates that the effect of the rotation rate on the strength of the FSP samples was complicated, and it could not be simply concluded from the effect of the heat input or particle break-up. After post-FSP artificial aging, the higher rotation rate produced a slightly higher strength, which was attributed to the high heat input promoting the dissolution of the coarse Mg_2Si particles, which were reprecipitated during the subsequent artificial aging.

Ogris *et al.*[33] indicated that the fine rounded Si particles would significantly increase the elongation of alloys. However, there was no discernible effect on the elongation from the evolution of the Si particle sizes when they became finer with an increasing rotation rate. Furthermore, after the post-FSP artificial aging, the elongation of the one-pass FSP sample of 1200/150 was the best, and at the same time the reduced value in elongation after aging was the least. This indicates that the elongation of the FSP samples was not determined by the size of the Si particles.

In group B, increasing the travel speed induced the decrease in the strain in a unit volume, and both the duration at higher temperatures and the preheating time in a thermal cycle were shortened. In this case, the deformation resistance of the material increased, resulting in an increase in the aspect ratio and roundness of the particles and the volume fraction of porosity However, the particle size was decreased with increasing the travel speed. It is noted that the tensile properties of the samples changed little as the travel speed changed either before or after artificial aging (Figure 9). Therefore, it could be concluded that changing the travel speed in a small range would not exert a significant effect on the tensile properties of A356 alloy.

D. *Effects of FSP Passes on Tensile Properties*

In group C, the single-pass FSP sample (sample C1) showed much better tensile properties than the BM (Table II; Figure 10(a)), and the 2-pass FSP sample

(sample C2) was obviously better than the single-pass one. However, the further increment of FSP passes only slightly increased the strength of the FSP samples (Figure 10(a)). This can be explained as follows. During the first pass FSP, severe plastic deformation with thermal exposure broke up the coarse eutectic silicon particles and distributed them homogeneously, and eliminated porosity, leading to large mechanical property improvement. When increasing FSP to two passes, further microstructural refinement, homogenization, and densification were achieved, thereby producing better mechanical properties than the single-pass FSP. Similar results were reported by Ma *et al*.[22] When further increasing FSP to more than 2 passes, the strain and strain rate of deformation resulting from FSP could not further apparently modify the microstructure. As a result, the microstructure of the FSP samples did not show obvious differences based on metallographic observations (Figure 4) and the detailed statistical measurements on the size and the roundness of the particles (Figure 5; Table IV). Consequently, there is a law of diminishing returns with regard to the multi-pass FSP for microstructural modification and mechanical property improvement.

In general, the multi-pass FSP resulted in a slight accumulative increase of dissolved Mg atoms to some extent, therefore more β''-Mg_2Si precipitated during the post-FSP aging. As shown in Figure 6, 2-pass FSP produced more precipitation of β''-Mg_2Si after the post-FSP artificial aging than single-pass FSP. Therefore, the strength of the 2-pass FSP sample increased significantly compared with that of the single-pass FSP sample, which is in agreement with that reported by Ma *et al*.[22] However, with a further increase of the number of FSP passes to five passes in the present study, the precipitate peak of β''-Mg_2Si was only slightly higher than that of the 2-pass FSP sample. This indicates that the FSP with more than two passes did not significantly increase the amount of dissolved Mg atoms. In this case, further increasing the number of FSP passes beyond two passes could not significantly increase the strength.

Recently, Tutunchilar *et al*.[28] reported that in a multi-pass FSP of LM13 eutectic Al-Si as-cast alloy, from 1 pass to 4 passes, the uniform elongation of the FSP samples did not increase consistently with increasing FSP passes. Similarly, the uniform elongation in group C did not change much with an increase in the number of FSP passes, despite finer and more uniformly distributed Si particles following more FSP passes. It is noted that the total elongation had a peak for the three-pass FSP sample before the aging, and for the four-pass FSP sample after the aging. Such a variation trend indicated that the ductility of the FSP samples was changed by increasing FSP passes.

In group D, 2-pass FSP with different FSP directions was conducted. In general, the advancing and retreating sides of the SZ were not symmetrical in the FSP samples. Reversing the travel direction of the second pass would mix two different deformation microstructures on the advancing and retreating sides with different orders. The micrographic observations did not show significant differences between the two samples, and the detailed statistical measurements showed that the size and the roundness of the particles were similar. As shown in Figure 11, the 2-pass FSP sample with the opposite direction showed slightly lower strength and higher elongation than its counterpart, but it showed higher tensile properties than its counterpart after the post-FSP artificial aging. As discussed above, the microstructure between the two samples had no significant difference; therefore, the Mg_2Si might be the effective strengthening factor, and its content may vary slightly with the deformation temperature during the 2nd pass FSP.

V. CONCLUSIONS

1. FSP on cast A356 alloy not only eliminated most of the porosity but also broke up and dispersed the bulky Si particles, Fe-rich phases, and Mg_2Si particles; moreover, it dissolved most of the Mg_2Si particles.
2. Increasing the rotation rate would effectively break-up the particles, but it contributed little to the elimination of porosity. Increasing the travel speed did not change the size of the particles, but the size and volume fraction of porosity increased slightly.
3. Single-pass FSP can effectively enhance the ductility and strength of the BM without generating a significant strength difference among the various FSP parameters. With increasing the rotation rate at a fixed travel speed, the tensile properties of the FSP samples did not change much; however, after the artificial aging, the strength increased following an increase of the rotation rate. By increasing the travel speed at a fixed rotation rate, the tensile properties changed little, even after the artificial aging.
4. For the multi-pass FSP, the 2-pass FSP sample exhibited an obvious advantage in the microstructure modification and tensile properties compared with the single-pass sample. The 2-pass FSP with rotation rate/travel speed of 1500/300 was determined to be the optimal parameter combination for producing the best mechanical properties. A further increase in the number of FSP passes only resulted in a slight improvement in the microstructure and tensile properties of the FSP samples.
5. For the 2-pass FSP, the direction of the second FSP did not show a distinct effect on the microstructure and tensile properties of the FSP samples, but the opposite direction might be more effective than the same direction on the elimination of porosity.

ACKNOWLEDGMENTS

The authors gratefully acknowledge the support of the National Natural Science Foundation of China under Grant No. 51331008.

NOMENCLATURE

FSP Friction stir processing
FSW Friction stir welding

BM	Base material
SZ	Stirred zone
DSC	Differential scanning calorimeter
SEM	Scanning electron microscopy
YS	Yield strength
UTS	Ultimate tensile strength
UEL	Uniform elongation
EL	Elongation
OD	Opposite direction

REFERENCES

1. K.T. Kashyap, S. Murali, K.S. Raman, and K.S.S. Murthy: *Mater. Sci. Technol.*, 1994, vol. 9, pp. 189–203.
2. M.H. Lee, J.J. Kim, K.H. Kim, N.J. Kim, S. Lee, and E.W. Lee: *Mater. Sci. Eng. A*, 2003, vol. 340, pp. 123–29.
3. D.L. Zhang and L. Zheng: *Metall. Mater. Trans. A*, 1996, vol. 27A, pp. 3983–91.
4. Q.G. Wang and C.H. Caceres: *Mater. Sci. Eng. A*, 1998, vol. 241, pp. 72–82.
5. M.E. Seniw, J.G. Conley, and M.E. Fine: *Mater. Sci. Eng. A*, 2000, vol. 285, pp. 43–48.
6. M.K. Surappa, E. Blank, and J.C. Jaquet: *Scripta Metall.*, 1986, vol. 20, pp. 1281–86.
7. G. Atxaga, A. Pelayo, and A.M. Irisarri: *Mater. Sci. Technol.*, 2001, vol. 17, pp. 446–50.
8. S. Kumai, J. Hu, Y. Higo, and S. Nunomura: *Acta Mater.*, 1996, vol. 44, pp. 2249–57.
9. M.E. Seniw, J.G. Conley, and M.E. Fine: *NSF Symposium on Micromechanic Modeling of Industrial Materials*, Elsevier Science SA, Seattle, WA, 1998, pp. 43–48.
10. W.W. Bose-Filho, E.R. de Freitas, V.F. da Silva, M.T. Milan, and D. Spinelli: *Int. J. Fatigue*, 2007, vol. 29, pp. 1846–54.
11. H.R. Ammar, A.M. Samuel, and F.H. Samuel: *Mater. Sci. Eng. A*, 2008, vol. 473, pp. 65–75.
12. F.M. Al-Kharafi and W.A. Badawy: *Electrochim. Acta*, 1995, vol. 40, pp. 1811–17.
13. J. Quaresma, C. Santos, and A. Garcia: *Metall. Mater. Trans. A*, 2000, vol. 31A, pp. 3167–78.
14. P.R. Goulart, J.E. Spinelli, W.R. Osóio, and A. Garcia: *Mater. Sci. Eng. A*, 2006, vol. 421, pp. 245–53.
15. K. Lee, Y.N. Kwon, and S. Lee: *J. Alloy. Compd.*, 2008, vol. 461, pp. 532–41.
16. L.B. Wang and S. Shivkumar: *Z. Metallk.*, 1995, vol. 86, pp. 441–45.
17. T.J. Hurley and R.G. Atkinson: *Giessereipraxis*, 1987, pp. 1–7.
18. W.M. Thomas, E.D. Nicholas, J.C. Needham, M.G. Murch, P. Templesmith, and C.J. Dawes: G.B. Patent Application No. 9125978.8, 1991.
19. W.B. Lee, Y.M. Yeon, and S.B. Jung: *Mater. Sci. Eng. A*, 2003, vol. 355, pp. 154–59.
20. Z.Y. Ma, R.S. Mishra, and M.W. Mahoney: *Scripta Mater.*, 2004, vol. 50, pp. 931–35.
21. S.R. Sharma, Z.Y. Ma, and R.S. Mishra: *Scripta Mater.*, 2004, vol. 51, pp. 237–41.
22. Z.Y. Ma, S.R. Sharma, and R.S. Mishra: *Metall. Mater. Trans. A*, 2006, vol. 37A, pp. 3323–36.
23. Z.Y. Ma, S.R. Sharma, and R.S. Mishra: *Mater. Sci. Eng. A*, 2006, vol. 433, pp. 269–78.
24. Z.Y. Ma, A.L. Pilchak, M.C. Juhas, and J.C. Williams: *Scripta Mater.*, 2008, vol. 58, pp. 361–66.
25. S. Jana, R.S. Mishra, J.B. Baumann, and G. Grant: *Scripta Mater.*, 2009, vol. 61, pp. 992–95.
26. L. Karthikeyan, V.S. Senthilkumar, and K.A. Padmanabhan: *Mater. Des.*, 2010, vol. 31, pp. 761–71.
27. N. Sun and D. Apelian: *JOM*, 2011, vol. 63, pp. 44–50.
28. S. Tutunchilar, M.K. Besharati Givi, M. Haghpanahi, and P. Asadi: *Mater. Sci. Eng. A*, 2012, vol. 534, pp. 557–67.
29. S.A. Alidokht, A. Abdollah-zadeh, S. Soleymani, T. Saeid, and H. Assadi: *Mater. Charact.*, 2012, vol. 63, pp. 90–97.
30. T.S. Mahmoud, O.M. Shaban, H.M. Zakaria, and T.A. Khalifa: *Mater. Sci. Technol.*, 2010, vol. 26, pp. 1120–24.
31. M.W. Mahoney, C.G. Rhodes, J.G. Flintoff, R.A. Spurling, and W.H. Bingel: *Metall. Mater. Trans. A*, 1998, vol. 29A, pp. 1955–64.
32. Y.S. Sato, M. Urata, H. Kokawa, and K. Ikeda: *Mater. Sci. Eng. A*, 2003, vol. 354, pp. 298–305.
33. E. Ogris, A. Wahlen, H. Lühinger, and P.J. Uggowitzer: *J. Light Met.*, 2002, vol. 2, pp. 263–69.